Measurement of ^{129}Xe frequency shift due to Cs–^{129}Xe collisions*

Fang Jian-Cheng(房建成), Wan Shuang-Ai(万双爱)†, and Chen Yao(陈 瑶)

School of Instrument Science and Opto-Electronics Engineering, Beihang University, Beijing 100191, *China*

(Received 27 December 2013; revised manuscript received 14 February 2014; published online 10 April 2014)

Enhancement factor κ_0, which characterizes NMR and EPR frequency shifts for Cs–^{129}Xe, is measured for the first time. The enhancement factor κ_0 was measured to be (702±41) at 80 °C and (653±20) at 90 °C, using the NMR frequency shift, detected by atomic magnetometer at a low magnetic field of 100 nT. This result is useful for predicting the EPR frequency shifts for Cs and the NMR frequency shifts for ^{129}Xe in spin-exchange cells.

Keywords: Cs–^{129}Xe, frequency shift, atomic magnetometer

PACS: 34.10.+x, 85.70.–w, 85.60.–q **DOI:** 10.1088/1674-1056/23/6/063401

1. Introduction

Hyperpolarized ^{129}Xe has been exploited for a variety of scientific and medical applications, such as searches for permanent electric dipole moment in atoms,[1–3] CPT violation experiments,[4–6] nuclear magnetic field compensation in the nuclear spin gyroscopes,[7] and medical imaging.[8,9] A common technique for producing large quantities of hyperpolarized ^{129}Xe is spin-exchange optical pumping (SEOP), and Cs is the best choice for SEOP.[10–12] The Fermi-contact hyperfine interaction $\alpha(R)K\cdot S$ between the noble-gas nuclear spin K and the alkali-metal electron spin S is a fundamental aspect of SEOP. This interaction gives rise to complementary shifts in both the NMR frequency of the noble gas and the EPR frequency of the alkali-metal, and it can be well-described by effective magnetic fields with the appropriate enhancement factors:[13]

$$\delta B_{\rm a}^z = \frac{8\pi}{3}\frac{\mu_K}{K}\kappa_{\rm ab} n_{\rm b}\langle Kz\rangle, \tag{1}$$

$$\delta B_{\rm b}^z = -\frac{8\pi}{3} g_{\rm s}\mu_{\rm B}\kappa_{\rm ba} n_{\rm a}\langle Sz\rangle, \tag{2}$$

where $\delta B_{\rm a}^z$, $\delta B_{\rm b}^z$ are the equivalent static magnetic fields caused by the alkali-metal electron spins and the noble-gas nuclear spins, respectively; $n_{\rm a}$ and $n_{\rm b}$ are the number density of alkali-metal atoms and noble-gas atoms, respectively; $\langle Kz\rangle$, $\langle Sz\rangle$ are the expectation values of longitudinal components of the noble-gas nuclear and alkali-metal electron spins, respectively; $\kappa_{\rm ab}$ and $\kappa_{\rm ba}$ are the enhancement factors, which contain contributions from alkali-metal–noble-gas binary collisions κ_0 and three-body collisional breakup of van der Waals molecules κ_1. Noble-gas or the third body gas pressures above one atmosphere will decrease the lifetime of van der Waals molecules, so that the enhancement factors $\kappa_{\rm ab}$ and $\kappa_{\rm ba}$ converge to a single value, κ_0.

In applications of hyperpolarized ^{129}Xe, it is important to have an accurate measurement of ^{129}Xe polarization. A convenient tool for this purpose is the measurement of complementary shift in the EPR frequency of Cs, but to date that has been no published measurement of the Cs–^{129}Xe enhancement factor κ_0. In this paper, we present the first such measurement of κ_0 for Cs–^{129}Xe. Previous measurements of κ_0 for alkali-metal–noble-gas pairs, which used EPR frequency shift at high magnetic fields of several Gs (1 Gs = 10^{-4} T) or T, are listed in Table 1.[13–18] Here, we investigate a different method to measure κ_0 for Cs–^{129}Xe, which is to use the NMR frequency shift detected by an atomic magnetometer at a low magnetic field of 100 nT.

According to Eqs. (1) and (2), the Fermi-contact interaction in the Cs–^{129}Xe system results in an effective magnetic field experienced by the ^{129}Xe atoms, which is given by

$$\delta B_{\rm Xe}^z = \frac{8\pi}{6} g_{\rm s}\mu_{\rm B}\kappa_{\rm ba} n_{\rm Cs} P_{\rm Cs}^z, \tag{3}$$

where $g_{\rm s}$ is the electron's g factor, $\mu_{\rm B}$ is the Bohr magneton, and $P_{\rm Cs}^z = 2\langle Sz\rangle_{\rm Cs}$ is the cesium polarization. In a high-density alkali-metal cell, this field causes the precession shift of ^{129}Xe atoms, and this shift can be detected by the atomic magnetometer. So we can measure the ^{129}Xe atoms' precession frequency shift as a function of the cesium polarization. In accordance with Eq. (3), the frequency shift is proportional to the cesium polarization. Therefore, the enhancement factor $\kappa_{\rm ba}$ is proportional to the slope of the experimentally determined plot of precession frequency shift versus cesium polarization, which can be described as

$$\kappa_{\rm ba} = \frac{\Delta\omega}{P_{\rm Cs}^z}\cdot\frac{6}{8\pi\gamma_{\rm n} g_{\rm s}\mu_{\rm B} n_{\rm Cs}}, \tag{4}$$

where $\gamma_{\rm n}$ is the gyro-magnetic ratio of the ^{129}Xe nuclei. In our experiment, the pressure in the cell is above one atmosphere, so the enhancement factor $\kappa_{\rm ba}$ converges a single value of κ_0.

*Project supported by the Key Program of the National Natural Science Foundation of China (Grant Nos. 61227902, 61273067, and 6137210) and SAST Foundation of China.

†Corresponding author. E-mail: sawan@aspe.buaa.edu.cn

© 2014 Chinese Physical Society and IOP Publishing Ltd

Table 1. Summary of previously published enhancement factor measurements and that presented in this paper. The published measurements are marked by reference numbers, and our present measurement is marked by $\surd$.

Pair	κ_0
K–^{3}He	5.9[14]
Rb–^{3}He	4.52[15]
Rb–^{83}Kr	270±95[13]
Rb–^{129}Xe	644±260,[11] 493±31[17]
Cs–^{129}Xe	$\surd$

2. Experiment setup and procedure

2.1. Experiment setup

The experimental setup is shown in Fig. 1 and is described elsewhere.[18–20] Two cubic glass cells with a side of 2 cm were each filled with a droplet of Cs metal, 20 torr of ^{129}Xe, 700 torr of N_2, and 50 torr (1 torr = 1.33322×10^2 Pa) of ^{129}Xe, 700 torr of N_2. The cells were placed in a non-magnetic oven and heated to 80 °C–90 °C by the flowing hot air. The oven was located inside a four-layer set of cylindrical magnetic shields with compensating magnetic coils, which were driven by a precision current source. The compensating magnetic coils were also used to apply magnetic fields to the cell. In the measurements described below, all three components of the magnetic field had been compensated to be close to zero to keep the system in the Spin-Exchange Relaxation-Free (SERF) regime.[18–20] Cs atoms were circularly polarized by the pump beam through a polarizer and a 1/4 wave plate along the z direction. ^{129}Xe atoms were polarized by spin-exchange collisions with polarized Cs atoms. A shutter was used to turn on/off the pump beam. A 1/2 wave plate and PBS were added to the basic setup to tune the intensity of the pump beam and to tune the cesium polarization. A linearly polarized probe beam passed through the glass cell orthogonal to the pump beam and measured the Cs atoms' spin polarization along the direction of propagation. The pump beam and the probe beam originated from two Sacher Lion external cavity diode laser (ECDL) systems and expanded to illuminate the whole cell.

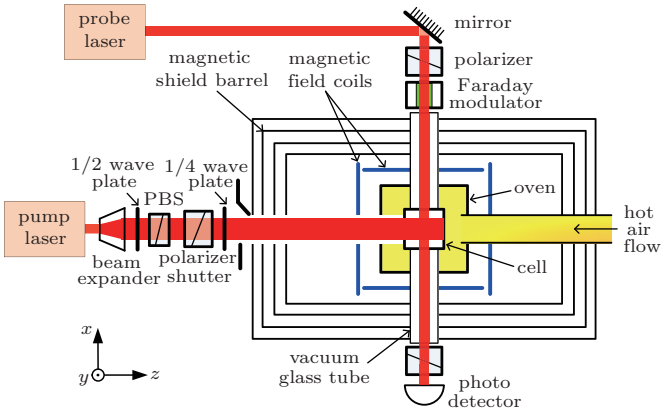


Fig. 1. (color online) Experimental setup.

2.2. Measurement of the cesium number density

We used an optical absorption method to measure the Cs number density in the cells. In an atomic vapor, for linearly polarized laser propagating along the z direction, the absorption of un-polarized photons follows Beer's law:

$$I(z) = I(0)\exp(-n\sigma(\upsilon)z), \tag{5}$$

where n is the number density of the alkali atoms, $\sigma(\upsilon)$ is the frequency-dependent cross section, z is the position in the cell and $I(0)$ is the intensity of the laser where it enters the front of the cell.

The number density can be given by

$$n = \frac{1}{\sigma(\upsilon)\cdot l}\ln\frac{I(0)}{I(l)}, \tag{6}$$

where l is the length of the cell and $I(l)$ is the intensity of laser as it is transmitted through the cell.

The frequency-dependent cross section of Cs can be calculated by

$$\begin{aligned}\sigma(\upsilon) = r_e c f\Bigg(&\frac{7}{64}\frac{\Gamma/2}{(\upsilon-\upsilon_{33})^2+(\Gamma/2)^2}\\ &+\frac{21}{64}\frac{\Gamma/2}{(\upsilon-\upsilon_{34})^2+(\Gamma/2)^2}\\ &+\frac{21}{64}\frac{\Gamma/2}{(\upsilon-\upsilon_{43})^2+(\Gamma/2)^2}\\ &+\frac{15}{64}\frac{\Gamma/2}{(\upsilon-\upsilon_{44})^2+(\Gamma/2)^2}\Bigg),\end{aligned} \tag{7}$$

where c is the speed of light, r_e is the classical electron radius, $f = 1/3$ is the oscillator strength of the transition, Γ is the full-width at half maximum, υ is the pump laser frequency, and υ_{33}, υ_{34}, υ_{43}, and υ_{44} are the resonance frequencies of the four transitions $6^2S_{1/2}$, F = 3→$6^2P_{1/2}$, F = 3, $6^2S_{1/2}$, F = 3→$6^2P_{1/2}$, F = 4, $6^2S_{1/2}$, F = 4→$6^2P_{1/2}$, F = 3, and $6^2S_{1/2}$, F = 4→$6^2P_{1/2}$, F = 4, respectively.

In our experiment, we first used linearly polarized light near the D1 line of Cs to measure the intensities $I(0)$ and $I(l)$. Furthermore, the density of Cs can be determined in accordance with Eqs. (5)–(7).

2.3. Measurement of the cesium polarization

Through optical pumping, the equilibrium polarization of Cs along the z direction becomes

$$P_{\rm Cs}^z = \frac{R_{\rm p}}{R_{\rm p}+R_{\rm rex}}\cos\theta\cdot\boldsymbol{s}_{\rm p}\cdot\hat{z} = \frac{R_{\rm p}}{R_{\rm tot}}\cos^2\theta, \tag{8}$$

where $R_{\rm p}$ is the pumping rate, $R_{\rm rex}$ is the spin-relaxation of the electron, $R_{\rm tot}$ is the total spin-relaxation of the electron including the pumping rate $R_{\rm p}$ and the spin-relaxation rate $R_{\rm rex}$. $\boldsymbol{s}_{\rm p}$ is the circular polarization degree of the pump laser, θ is the angle between the direction of pump laser propagation and the

applied magnetic field, and $\theta \approx 0$ in our work. Equation (8) then becomes

$$P_{\rm Cs}^z = \frac{R_{\rm p}}{R_{\rm tot}}. \tag{9}$$

The pumping rate is related to the intensity of the light I as

$$R_{\rm p} = I\frac{\sigma(\upsilon)}{h\upsilon}, \tag{10}$$

where $\sigma(\upsilon)$ is the frequency-dependent cross section, h is the Planck constant and υ is the frequency of the pump laser. And, therefore, the total relaxation rate $R_{\rm tot}$ can be described by

$$R_{\rm tot} = R_{\rm p} + R_{\rm rex} = I\frac{\sigma(\upsilon)}{h\upsilon} + R_{\rm rex} = K_0 \cdot I + R_{\rm rex}, \tag{11}$$

where we define $K_0 = \sigma(\upsilon)/h\upsilon$ to simplify the relation between $R_{\rm tot}$ and I.

In accordance with Eqs. (8)–(11), in order to measure the Cs polarization, we can measure the total relaxation rate $R_{\rm tot}$ as a function of the pump intensity, and then extrapolate the spin-relaxation rate $R_{\rm rex}$, where the pump beam intensity is zero. The pumping rate and the polarization of Cs are ultimately determined in accordance with Eq. (9).

The measurement of the total relaxation rate $R_{\rm tot}$ was carried out on a time scale that is short compared to the Cs–^{129}Xe spin-exchange rate, such that the ^{129}Xe polarization was negligibly small. Simultaneously, a small static magnetic field of 16 nT along the y direction and a variational magnetic field from -2000 nT to 2000 nT along the z direction were applied using compensation magnetic coils. Under these conditions, the behavior of the system can be well-described by a Bloch equation:[18,21]

$$\frac{\partial \boldsymbol{P}_{\rm Cs}}{\partial t} = \frac{1}{Q(P_{\rm Cs})}(\gamma_{\rm e}\boldsymbol{B} \times \boldsymbol{P}_{\rm Cs} + R_{\rm p}\boldsymbol{s}_{\rm p} - R_{\rm tot}\boldsymbol{P}_{\rm Cs}), \tag{12}$$

where $\gamma_{\rm e}$ is the gyro-magnetic ratio of the electrons, and $Q(P_{\rm Cs}) \approx Q(P_{\rm Cs}^z)$ is the nuclear slow-down factor, which is calculated for nuclear spin $I = 7/2$:[22]

$$Q(P_{\rm Cs}^z) = \frac{2(P_{\rm Cs}^{z6} + 17P_{\rm Cs}^{z4} + 35P_{\rm Cs}^{z2} + 11)}{P_{\rm Cs}^{z6} + 7P_{\rm Cs}^{z4} + 7P_{\rm Cs}^{z2} + 1}. \tag{13}$$

The detected system signal comes from the projection of the spins along the x axis in our experiment. The steady state polarization along this direction is

$$P_{\rm Cs}^x = P_0\frac{kB_y + B_xB_z}{k^2 + B_x^2 + B_y^2 + B_z^2}, \tag{14}$$

where P_0 is the equilibrium electron spin polarization, and we introduce a parameter $k = R_{\rm tot}/\gamma_{\rm e}$. Equation (14) can be fit to the following function

$$y = a \cdot \frac{(x-b)\cdot e + c \cdot B_y}{(x-b)^2 + c^2 + e^2 + B_y^2} + d \tag{15}$$

to determine the total spin-relaxation $R_{\rm tot} = k \times \gamma_{\rm e}$, and to extrapolate the spin-relaxation rate $R_{\rm rex}$ where the pump beam intensity is zero.

In conclusion, the equilibrium polarizations of Cs along the z direction $P_{\rm Cs}^z$ at each pump intensity are ultimately determined in accordance with Eqs. (8), (9), and (11).

2.4. Measurement of ^{129}Xe precession frequency shift

In previous measurements, the alkali-metal electron spins and the noble-gas nuclear spins are decoupled from each other at high magnetic field.[11–15] Therefore, the equations describing the electron and nuclear spins' polarization dynamics can be considered separately, simplifying the problem considerably. In our experiment, Cs and ^{129}Xe atoms are located at an ultralow magnetic field of about 100 nT, such that the frequency shifts due to spin-exchange are comparable with or larger than the Larmor frequencies. This leads to a hybrid oscillation frequency contributed from both Cs and ^{129}Xe spins for small transverse excitations of the spins. The hybrid oscillation frequency is monitored through $P_{\rm Cs}^x$ and can be solved by the following system of coupled Bloch equations (16) for Cs and ^{129}Xe:[5]

$$\begin{aligned}
\frac{\partial \boldsymbol{P}_{\rm Cs}}{\partial t} &= \frac{\gamma_{\rm e}}{Q(P_{\rm Cs})}(\boldsymbol{B} + \delta\boldsymbol{B}_{\rm Cs}) \times \boldsymbol{P}_{\rm Cs} \\
&\quad + R_{\rm tot}(P_{\rm e}^0\boldsymbol{z} - \boldsymbol{P}_{\rm Cs})/Q(P_{\rm Cs}), \\
\frac{\partial \boldsymbol{P}_{\rm Xe}}{\partial t} &= \gamma_{\rm n}(\boldsymbol{B} + \delta\boldsymbol{B}_{\rm Xe}) \times \boldsymbol{P}_{\rm Xe} + R_{\rm tot}^{\rm n}(P_{\rm n}^0\boldsymbol{z} - \boldsymbol{P}_{\rm Xe}),
\end{aligned} \tag{16}$$

where $\boldsymbol{P}_{\rm Xe}$ is the polarization of ^{129}Xe nuclear spin; $P_{\rm e}^0$, $P_{\rm n}^0$ are the equilibrium polarizations for the Cs and ^{129}Xe spins respectively; $\gamma_{\rm n}$ is the gyro-magnetic ratio of the ^{129}Xe nuclei; $R_{\rm tot}^{\rm n}$ is the total spin-relaxation of the ^{129}Xe nuclei;

$$\delta\boldsymbol{B}_{\rm Cs} = \frac{8\pi}{6}\mu_{\rm Xe}\kappa_0 n_{\rm Xe}\boldsymbol{P}_{\rm Xe}$$

is the enhancement magnetic field for Cs spins; and

$$\delta\boldsymbol{B}_{\rm Xe} = -\frac{8\pi}{6}g_{\rm s}\mu_{\rm B}\kappa_0 n_{\rm Cs}\boldsymbol{P}_{\rm Cs}$$

is the enhancement magnetic field for ^{129}Xe spins. Other parameters have been defined in Subsection 2.3.

Solving Eq. (16) with the reasonable approximation $R_{\rm tot}^{\rm n} \ll R_{\rm tot}$, the solution $P_{\rm Cs}^x$ measured by the polarized probe beam in our experiment is given by

$$\begin{aligned}
P_{\rm Cs}^x &= P_1 \exp\left[\left(-\frac{R_{\rm tot}}{Q(P_{\rm Cs})} + \frac{\gamma_{\rm e}\cdot\gamma_{\rm n}\cdot\delta B_{\rm Cs}^z\cdot\delta B_{\rm Xe}^z}{R_{\rm tot}}\right)t\right]\cos\omega_{\rm e}t \\
&\quad + P_2 \exp\left[\left(-\frac{1}{2}R_{\rm tot}^{\rm n} - \frac{\gamma_{\rm e}\cdot\gamma_{\rm n}\cdot\delta B_{\rm Cs}^z\cdot\delta B_{\rm Xe}^z}{R_{\rm tot}}\right)t\right]\cos\omega_{\rm n}t, \\
\omega_{\rm e} &= \frac{\gamma_{\rm e}}{Q(P_{\rm Cs})}(B_z + \delta B_{\rm Cs}^z), \\
\omega_{\rm n} &= \gamma_{\rm n}(B_z + \delta B_{\rm Xe}^z),
\end{aligned} \tag{17}$$

where P_1 and P_2 depend on the initial conditions; and ω_e and ω_n are the precession frequencies of Cs and ^{129}Xe spins, respectively.

In our experiment, the measurement of ^{129}Xe precession frequency was followed the measurement of Cs polarization. After measuring Cs polarization, an external magnetic field B_z of about 100 nT was applied along the z direction and the shutter was opened to polarize ^{129}Xe by spin-exchange collisions with the polarized Cs atoms. To measure the precession frequency of ^{129}Xe spins, we measured the transient response P^x_{Cs} of the system, following a small pulse magnetic field along the y direction. The transient responses can be fitted based on Eq. (17). The faster oscillations correspond to the precession of the Cs electrons, while the slow oscillations correspond to the precession of the ^{129}Xe. From Eq. (17), we know that the detected precession frequency of the ^{129}Xe is contributed from not only the enhancement magnetic field introduced by Cs spins, but also the external magnetic field B_z. Indeed, the direction of magnetic field δB^z_{Xe}, introduced by Cs spins is along the propagating direction of the pump beam, and the sign depends on the sign of circular polarization. To measure the ^{129}Xe atoms precession frequency shift due to δB^z_{Xe}, we first set the pump beam on the left-circular and measured the ^{129}Xe precession frequency ω_{n1}, and then set the pump beam on the right-circular and measured the ^{129}Xe precession frequency ω_{n2} under the same condition as the left-circular. Frequencies ω_{n1} and ω_{n2} are given by

$$\omega_{n1} = \gamma_n(B_z + \delta B^z_{Xe}), \tag{18}$$

$$\omega_{n2} = \gamma_n(B_z - \delta B^z_{Xe}). \tag{19}$$

The ^{129}Xe atoms' precession frequency shift due to δB^z_{Xe} can be given directly by the difference between these two frequencies:

$$\Delta\omega = \gamma_n \cdot \delta B^z_{Xe} = \frac{1}{2}(\omega_{n1} - \omega_{n2}). \tag{20}$$

3. Results and error analysis

We first measured the intensities $I(0)$ and $I(l)$ three times, using linearly polarized laser light on the resonance frequency of the transition. The results are listed in Table 2. The cells used in our experiment were filled with quenching gases and, therefore, the linewidth Γ was mainly contributed from pressure broadening. The pressure broadening of Cs in an N_2 environment is $\Gamma_{N_2} = 14.83$ GHz/amg. Thus, the line width Γ in our experiment was given by

$$\begin{aligned}\Gamma &= 14.83 \times 10^9 \text{ Hz/amg} \times \frac{700 \text{ torr}}{760 \text{ torr/amg}} \\ &= 14.83 \times 10^9 \text{ Hz}.\end{aligned} \tag{21}$$

When the linewidth is large compared to the hyperfine splitting, the individual transitions are unresolved and only a single transition is observed. Thus, equation (7) becomes

$$\sigma(\upsilon) = r_e c f \frac{\Gamma/2}{(\upsilon - \upsilon_0)^2 + (\Gamma/2)^2} \tag{22}$$

and can be simplified as

$$\sigma(\upsilon) = \frac{2 r_e c f}{\Gamma} = 4.129 \times 10^{-13} \text{cm}^2, \tag{23}$$

when the frequency of the laser is on-resonance.

According to Eq. (23), Eq. (6), and the measured intensities $I(0)$ and $I(l)$, the number densities of Cs were [Cs]=(1.69±0.015)×10^{12} cm^{-3} for the NO. 1 cell at 80 °C and [Cs]= (3.58±0.019)×10^{12} cm^{-3} for the NO. 2 cell at 90 °C, about half the saturated vapor pressure. This happened because the temperature sensor is external to the cell and measures the temperature at a single location; however, the coldest region of the cell determines the alkali density. In addition, there are a number of surface effects that allow alkali atoms to be adsorbed into the glass, thereby lowering the effective density at a given temperature.

Table 2. Experimentally measured values of $I(0)$, $I(l)$, and the density of Cs [Cs] calculated according to Eq. (6); $I(0)$ is the laser intensity entering the front of the cell, and $I(l)$ is the intensity of laser transmitted through the cell.

NO.	P(Xe)/torr	P(N_2)/torr	Temperature of the cell surface/ ° C	$I(0)$/mW	$I(l)$/mW	[Cs] /cm^{-3}
1	20	760	80	92	22.5	(1.69±0.015)×10^{12}
				244	60.8	
				317	78.6	
2	50	760	90	250	13.8	(3.49±0.017)×10^{12}
				418	23.2	
				630	35.4	

Figure 2 is a plot of the experimentally measured system's signal as a function of magnetic field B_z for the five pump beam intensities. We fitted the data in accordance with Eqs. (14) and (15). There were five free parameters in each fit. The coefficient of determination and the standard error of the fit are listed in Table 3. From Table 3, it is clear that the coefficient of determination of the fit is above 99%, and the estimated errors in the extracted values R_{tot} are within ±3%.

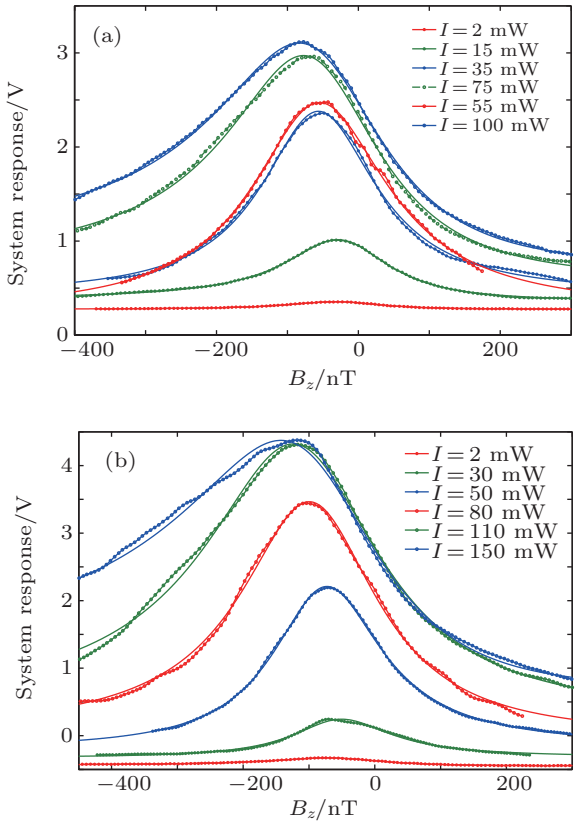


Fig. 2. (color online) Measured system's signal for two cells as a function of magnetic field B_z for the five intensities of the pump beam listed in Table 3. The solid lines overlaying the data are fits described in the text. Panel (a) cell NO. 1 at 80 °C, (b) cell NO. 2 at 90 °C.

Figure 3 is a plot of the measured $R_{\rm tot}$ versus the pump beam intensity according to Fig. 2. From the fitting result, the spin-relaxation rates $R_{\rm rex}$ at the pump beam intensity $I = 0$ were (13511±211) s^{-1} for the NO. 1 cell at 80 °C and (14730±433) s^{-1} for the NO. 2 cell at 90 °C, respectively. The values of polarization $P^z_{\rm Cs}$, extracted according to Eqs. (8) and (9), are listed in Table 3, and the estimated errors are within ±8%.

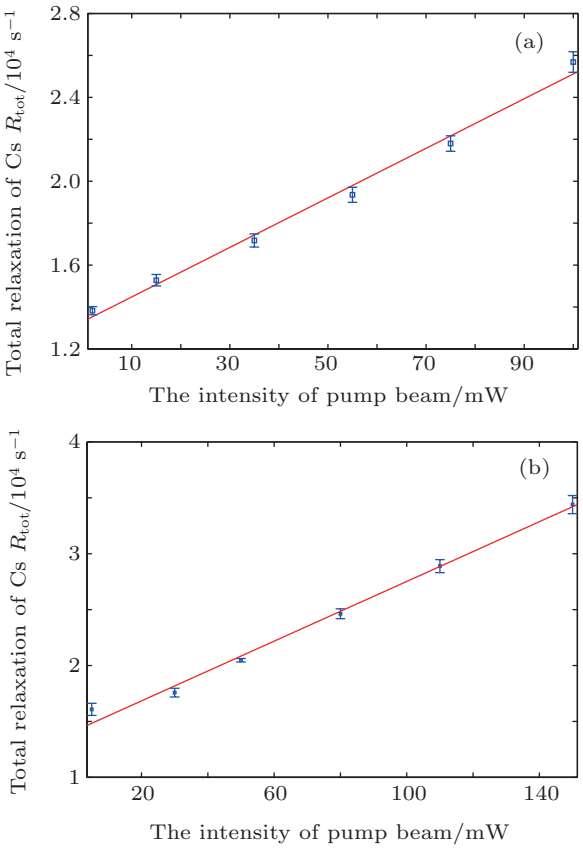


Fig. 3. (color online) The total relaxation $R_{\rm tot}$ versus the pump beam intensity. The spin-relaxation rate $R_{\rm rex}$ is the value at $I = 0$. Panel (a) cell NO. 1 at 80 °C, (b) cell NO. 2 at 90 °C.

Table 3(a). Experimentally measured values of $R_{\rm tot}$ and $P^z_{\rm Cs}$ for cell NO. 1 at different pump beam intensities at 80 °C.

Pump beam intensity/mW	The coefficient of determination of the fit	The standard error of the fit	Extracted relaxation rate $R_{\rm tot}/s^{-1}$	Polarization $P^z_{\rm Cs}$
2	99.88%	0.006	13824±195	0.023±0.002
15	99.89%	0.023	15277±274	0.116±0.002
35	99.71%	0.001	17172±313	0.213±0.002
55	99.75%	0.029	19352±360	0.302±0.002
75	99.89%	0.022	21797±369	0.38±0.001
100	99.7%	0.03	25685±490	0.474±0.002

Table 3(b). Experimentally measured values of $R_{\rm tot}$ and $P^z_{\rm Cs}$ for cell NO. 2 at different pump beam intensities at 90 °C.

Pump beam intensity/mW	The coefficient of determination of the fit	The standard error of the fit	Extracted relaxation $R_{\rm tot}$ rate $R_{\rm tot}/(1/s)$	Polarization $P^z_{\rm Cs}$
5	99.14%	0.016	15140±443	0.026±0.002
30	99.67%	0.002	18230±387	0.15±0.018
50	99.94%	0.017	20470±158	0.28±0.012
80	99.73%	0.052	24630±440	0.402±0.005
110	99.7%	0.066	28887±580	0.49±0.004
150	99.6%	0.07	34393±809	0.571±0.003

Figure 4 shows the transient response P_{Cs}^{x} of the system followed by a small, sudden B_y field step. The data were well described by an exponentially decaying oscillation polynomial and they were well fitted based on Eq. (17). There were six free parameters in the fit, and the coefficient of determination and the standard error of the fit were 99.06% and 0.08, respectively. From the fit, we determined the slow oscillations corresponding to the precession of ^{129}Xe. The extracted values of ^{129}Xe precession frequencies were listed in Table 4. The estimated error of the ^{129}Xe precession frequencies was within $\pm 0.1\%$. In accordance with Eq. (20), we determined the ^{129}Xe precession frequency shift $\Delta\omega$ due to δB_{Xe}^{z}.

We plotted the ^{129}Xe precession frequency shift as a function of Cs polarization, as shown in Fig. 5. The error of the fits was within $\pm 5\%$. In accordance with Eq. (4), the frequency shift is proportional to the polarization of Cs atoms. From the slope of the fit, we determined the $\kappa_0 = (702 \pm 41)$ for the NO.1 cell at 80 °C and $\kappa_0 = (653 \pm 20)$ for the NO. 2 cell at 90 °C, both of which are in agreement with the calculated $\kappa_0 = 879$.[23]

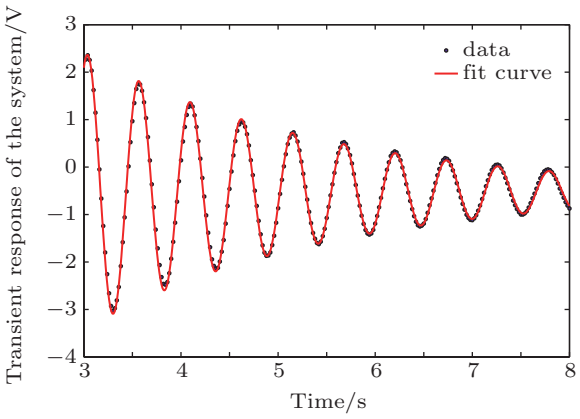


Fig. 4. (color online) Transient response P_{Cs}^{x} of system following a small, sudden step in the B_y field. The frequencies can be determined from the fit and are listed in Table 4.

Table 4(a). Experimentally measured values of ^{129}Xe precession frequencies for cell NO. 1 at different pump beam intensities at 80 °C.

Pump beam intensity/mW	^{129}Xe precession frequency/Hz		
	Left-circular ω_{n1}	Right-circular ω_{n2}	frequency shift $\Delta\omega$
15	1.951±0.001	1.925±0.001	0.013±0.001
35	1.961±0.002	1.915±0.001	0.023±0.0015
55	1.978±0.001	1.91±0.002	0.034±0.0015
75	1.979±0.002	1.897±0.002	0.041±0.002
100	1.996±0.001	1.894±0.001	0.051±0.001

Table 4(b). Experimentally measured values of ^{129}Xe precession frequencies for cell NO. 2 at different pump beam intensities at 90 °C.

Pump beam intensity/mW	^{129}Xe precession frequency/Hz		
	Left-circular ω_{n1}	Right-circular ω_{n2}	frequency shift $\Delta\omega$
30	1.967±0.002	1.906±0.002	0.0305±0.001
50	1.989±0.001	1.877±0.002	0.056±0.0015
80	1.996±0.001	1.832±0.002	0.082±0.0015
110	2.016±0.002	1.815±0.002	0.1005±0.001
150	2.043±0.003	1.806±0.001	0.1185±0.002

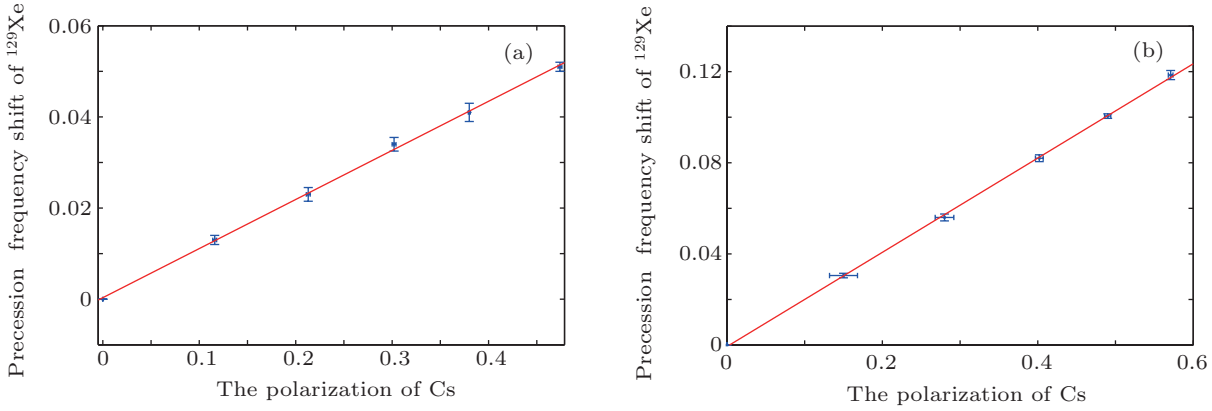


Fig. 5. (color online) The ^{129}Xe spin-precession frequency shift as a function of Cs polarization. The slopes of the fit, which are proportional to κ_0, are (0.1078±0.0053) Hz for the NO. 1 cell at 80 °C and (0.2069±0.0054) Hz for the NO. 2 cell at 90 °C. Panel (a) Cell NO. 1 at 80 °C, (b) Cell NO. 2 at 90 °C.

The sources of random error are the $R_{\rm tot}$ statistical error ($\pm 3\%$) and the ^{129}Xe precession frequency statistical error ($\pm 0.1\%$). These results stem mainly from the fluctuations of pump beam intensity and applied magnetic field. Possible systematic errors include: the measurement of the pump beam intensity, errors in the pump beam intensity dependence of temperature calibration, polarization calibration, and measurement of ^{129}Xe precession frequency shift due to drift of the applied magnetic field. To eliminate the error resulting from the drift of the applied magnetic field, we had all three components of the magnetic field compensated as close to zero as possible before the measurement of ^{129}Xe precession frequency every time. The compensation time was about 60 s and the residual magnetic field of strength was less than 0.02 nT after compensation, which was equal to 0.00023 Hz of ^{129}Xe precession frequency shift and systematic error within ($\pm 0.7\%$).

4. Conclusion

We measured the enhancement factor $\kappa_0 = (702 \pm 41)$ at 80 °C and $\kappa_0 = (653 \pm 20)$ at 90 °C for Cs–^{129}Xe, which is in agreement with the theoretical value of 879. As a result of the optical depth, the pump beam-provided Cs polarization was not uniform throughout the cell. Thus, the Cs polarization measured here was as an average, and therefore κ_0 measured here was as an average throughout the volume of the cell. It is worth noting that an additional geometric correction factor κ' should be included, which is smaller than 5% for nearly all geometries of interest for SEOP.[14] With the increasing interest in Cs and ^{129}Xe for SEOP, having robust and accurate measure of enhancement factor will be very important for future developments.

References

[1] Walker T G and Happer W 1997 *Rev. Mod. Phys.* **69** 629
[2] Vold T G, Raab F, Hecet B and Fortson E N 1984 *Phys. Rev. Lett.* **52** 2229
[3] Rosenberry M A and Chupp T E 2001 *Phys. Rev. Lett.* **86** 22
[4] Bear D, Stoner R E, Walsworth R L, Kostelecky V A and Lane C D 2000 *Phys. Rev. Lett.* **85** 5038
[5] Kornack T W and Romalis M V 2002 *Phys. Rev. Lett.* **89** 253002
[6] Smiciklas M, Brown J M, Cheuk L W, Smullin S J and Romalis M V 2011 *Phys. Rev. Lett.* **107** 171604
[7] Fang J C, Qin J, Wan S A, Chen Y and Li R J 2012 *Chin. Sci. Bull.* **58** 1512
[8] Newbury N R 1993 *Phys. Rev. A* **48** 558
[9] Yablonskiy D A, Sukstanskii A L, Woods J C, Gierada D S, Quirk J D, Hogg J C, Cooper J D and Conradi M S 2009 *J. Appl. Phys.* **107** 1258
[10] Jau Y Y, Kuzma N N and Happer W 2004 *Phys. Rev. A* **69** 061401
[11] Ni Z X, Shi Q C and Chen Z J 1998 *Chin. Phys.* **7** 481
[12] Zhang J C, Zhu Z L and Sun J F 2012 *Acta Phys. Sin.* **61** 093401 (in Chinese)
[13] Schaefer S R, Cates G D, Chien T R, Gonatas D, Happer W and Walker T G 1989 *Phys. Rev. A* **39** 11
[14] Babcock E, Nelson I A, Kadlecek S and Walker T G 2005 *Phys. Rev. A* **71** 013414
[15] Romalis M V and Cates G D 1998 *Phys. Rev. A* **58** 3004
[16] Barton A S, Newbury N R, Cates G D, Driehuys B, Middleton H and Saam B 1994 *Phys. Rev. A* **49** 2766
[17] Ma Z L, Sorte E G and Saam B 2011 *Phys. Rev. Lett.* **106** 193005
[18] Allred J C, Lyman R N, Kornack T W and Romalis M V 2002 *Phys. Rev. Lett.* **89** 130801
[19] Kominis I K, Kornack T W, Allred J C and Romalis M V 2003 *Nature* **422** 596
[20] Gusarov A, Levron D, Baranga B A, Paperno E and Shuker R 2011 *J. Appl. Phys.* **109** 07E507
[21] Seltzer S J and Romalis M V 2009 *Appl. Phys. Lett.* **85** 4804
[22] Ledbetter M P, Savukov I M, Acosta V M, Budker D and Romalis M V 2008 *Phys. Rev. A* **77** 033408
[23] Walker T G 1989 *Phys. Rev. A* **40** 9